

## Decoherence and Turbulence Sources in a Long Laser

Amy Roche and Svetlana Slepneva

*Department of Physical Sciences, Munster Technological University, Cork, Ireland*

Anton Kovalev 

*ITMO University, Birzhnevaya Liniya 14, 199034 St. Petersburg, Russia*

Alexander Pimenov and Andrei G. Vladimirov

*Weierstrass Institute, Mohrenstrasse 39, 10117 Berlin, Germany*

Massimo Giudici , Mathias Marconi, and Guillaume Huyet

*Université Côte d'Azur, CNRS, INPHYNI, 06200 Nice, France*

 (Received 28 December 2022; accepted 6 July 2023; published 1 August 2023)

We investigate the turn-on process in a laser cavity where the round-trip time is several orders of magnitude greater than the active medium timescales. In this long delay limit, we show that the universal evolution of the photon statistics from thermal to Poissonian distribution involves the emergence of power dropouts. While the largest number of these dropouts vanish after a few round-trips, some of them persist and seed coherent structures similar to dark solitons or Nozaki-Bekki holes described by the complex Ginzburg-Landau equation. These coherent structures connect stationary laser emission domains having different optical frequencies. Moreover, they emit intensity bursts which travel at a different speed, and, depending on the cavity dispersion sign, they may collide with other coherent structures, thus leading to an overall turbulent dynamics. The dynamics is well-modeled by delay differential equations from which we compute the laser coherence time evolution at each round-trip and quantify the decoherence induced by the collisions between coherent structures.

DOI: [10.1103/PhysRevLett.131.053801](https://doi.org/10.1103/PhysRevLett.131.053801)

The coherence property of light has fascinated researchers for several centuries, and, following the laser discovery, numerous devices have exploited coherence for applications in industries, ranging from communication networks to metrology. Examples include Mach-Zehnder modulators for optical communications [1], swept-source lasers for optical coherence tomography [2], optical frequency combs for high precision metrology [3], or ring laser gyroscopes with fractions of prad/s resolution, such as in the GINGER experiment [4–6].

The coherence properties of single mode lasers have been thoroughly investigated, whether in the stationary [7] or transient regimes [8]. Below the threshold, the photon statistics follow a thermal distribution, with the coherence time inversely proportional to the gain bandwidth. Above the threshold, the photon number is distributed according to Poisson statistics, and the coherence time is inversely proportional to the Schawlow-Townes linewidth [9]. Single-mode laser coherence has gained recent interest in the context of nanolasers where nontrivial photon statistics can emerge [10] and high spontaneous emission factors can be engineered, giving rise for example to thresholdless lasers [11].

In multimode lasers, the phase relationship between the active cavity modes is governed by the interplay between

dispersion and nonlinearities, which can lead to the generation of coherent structures or the emergence of fully decoherent outputs such as optical turbulence. Turbulence has been observed in the longitudinal dimension of multi-mode laser resonators where coherent structures such as dark solitons [12–14] or Nozaki-Bekki holes [15] have been studied. The analysis of optical turbulence has been recently transferred into the realm of integrated optics. In Ref. [16], it is shown that an integrated semiconductor ring laser can enter an optical frequency comb regime using a very low pumping power owing to phase turbulence, which arises from the phase-amplitude coupling of the laser field in the semiconductor material. Depending on the dispersion sign, the same device can also operate in the Nozaki-Bekki hole regime, as shown in Ref. [17]. While spatiotemporal laser instabilities are commonly modeled using partial differential equations (PDEs), such as the complex Ginzburg-Landau equation [16,18], the dynamics of long laser systems can be well modeled using delay differential equations (DDEs) [19,20]. The analogy between PDE and DDEs is discussed in Ref. [21]. In particular, it has been demonstrated that DDE models can exhibit localized structures [22–24], as well as convective [21], Eckhaus [25], and modulational [26] instabilities. In Ref. [26] it is

shown that a long-cavity laser displays a stable operation in the normal dispersion regime, while in the anomalous dispersion regime a modulational instability is observed. Coherent structures and turbulence have been thoroughly investigated in the stationary operation of long lasers above threshold [12,27]; however there is still little information available about the transition to turbulence in these lasers in the course of the turn-on transient when the pump parameter suddenly brings the laser above threshold.

This Letter aims to address this gap by providing an experimental and theoretical investigation of the dynamical and statistical properties of light during the turn-on transient of a highly multimode laser. Our study unveils the universal mechanisms that drive the evolution of a long laser from a stable, below-threshold operation, to a turbulent regime via the formation and collisions of coherent structures in the early round-trips of the transient buildup. Beyond laser physics, the emergence of coherent structures and turbulent states in the transient regime of dynamical systems has never been analyzed in detail. Our results provide an experimental and theoretical description about the buildup of these states which are typical in the complex Ginzburg-Landau equation and, therefore, are ubiquitous in nature.

Our laser system consists of a semiconductor gain medium enclosed in a passive fiber cavity whose round-trip is much larger than the timescale of the active medium. This long cavity allows unidirectional field propagation. Long cavity lasers are closely connected to Fourier domain mode-locked lasers [28] that are commonly used for optical coherence tomography. In particular, the setup considered in this Letter was used to describe the appearance of the modulational instability that limits the coherence of these light sources [29]. Thanks to the long ring cavity and the pointlike semiconductor gain medium, we are able to record and analyze during the laser turn-on the phase and intensity variations of the field within each round trip and to reconstruct the evolution of the coherence. Our results reveal that, during the first round-trips, the laser intensity buildup is characterized by the formation of power dropouts. After a few tens of round-trip, the largest number of these power dropouts disappear, and the photon statistics relaxes toward a Poisson statistics. However, few of them may survive and seed coherent structures similar to dark solitons or Nozaki-Bekki holes, as the ones described by the complex Ginzburg-Landau equation [30]. In the normal dispersion regime, these coherent structures, that we call *holes*, travel with a constant speed while their cores emit decaying intensity bursts that travel faster than the holes. In the anomalous dispersion regimes, the intensity bursts emitted by a hole can reach and alter the dynamics of the preceding hole and, as a result, lead to a chaotic trajectory of the holes. This interaction between holes, which is similar to defect-mediated turbulence, constitutes the main source for coherence degradation in long lasers operating in the anomalous dispersion regime.

The experimental setup is shown in Fig. 1. The laser includes a semiconductor optical amplifier (SOA) with a gain peak near 1.3  $\mu\text{m}$  and a tunable optical bandpass filter with 10 GHz transmission bandwidth. The total cavity length of about 21 m, corresponding to 104.32 ns cavity round-trip time was mostly comprised by the added lengths of the fiber pigtails of all the cavity components. In order to analyze the turn-on dynamics, the bias current  $I_b$  of the SOA is quickly turned on to the values of 1.2 or 1.6 times of its threshold current  $I_{\text{th}} = 92$  mA. The driver is quickly turned on by a square-shaped signal having a 20 ns rise time delivered by an arbitrary waveform generator. This time is much shorter than the laser cavity round-trip time. A 50/50 fiber splitter placed after the filter is used to extract the light out of the cavity (average output power is in the mW range), which is detected and monitored by a real-time oscilloscope with 12 GHz bandwidth, synchronously triggered by the same waveform generator. Using the interferometric technique described in Ref. [31], with the aid of a stable narrow linewidth laser, both the relative phase and the amplitude of the electric field of the laser are recorded in a single shot measurement, thus disclosing the evolution of the laser field within each round-trip of the laser turn-on. We describe the laser system shown in Fig. 1 with the DDE model developed in Ref. [29] and using the lumped element approach proposed in Ref. [20]. In order to take into account the dispersion of the optical fiber, a generalization of this model was developed in Ref. [26] that contains a distributed delay term together with an additional polarization equation. In the case of moderate dispersion, the distributed delay model can be approximated by a fixed delay model [32]. Here we use the rescaled version of the DDE laser model developed in Ref. [32]:

$$\begin{aligned} \gamma^{-1} \frac{dE(t)}{dt} + (1 - i\Delta)E(t) \\ = +A(t - \tau)[E(t - \tau) + \epsilon P(t - \tau)] + \beta(t), \end{aligned} \quad (1)$$

$$\frac{dP(t)}{dt} = -(\Gamma - i\Omega)P - E(t), \quad (2)$$

$$\gamma_g^{-1} \frac{dG(t)}{dt} = g_0 - G(t) - (e^{G(t)} - 1)|E(t) + \epsilon P(t)|^2 \quad (3)$$

with

$$A(t) = \sqrt{\kappa} \exp[(1 - i\alpha)G(t - \tau)/2] e^{i\varphi},$$

where  $t$  is the time,  $\tau$  is the cold cavity round-trip time,  $E(t)$  is the complex electric field envelope,  $G(t)$  is the gain,  $P(t)$  is the polarization of the optical fiber which can be tuned from normal to anomalous dispersion by changing the sign of  $\Omega$ ,  $\kappa$  describes the linear cavity losses,  $\gamma_g$  is the carrier density decay rate,  $g_0$  is the pump parameter,  $\alpha$  is the linewidth enhancement factor,  $\gamma$  is the filter bandwidth,  $\Delta$  is

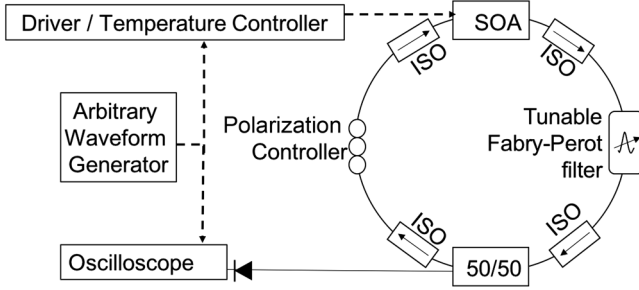


FIG. 1. Experimental setup of the semiconductor laser with a ring fiber cavity. ISO: fiber optical isolator. Half of the laser power is used for the detection.

the central frequency of the filter,  $\epsilon$  is the normalized dispersion strength, and  $\beta(t)$  is a white noise source with a variance of  $3.2 \times 10^{-3}$  during the first round-trip,  $t < \tau$ , and 0 afterward.  $\Gamma$  and  $\Omega$  are the polarization decay rate and frequency detuning. The parameter values used in the simulations were  $\tau = 104.32$  ns,  $\gamma = 19$  GHz,  $\gamma_g^{-1} = 1$  ns,  $\kappa = 0.036$  (corresponding to  $-14.5$  dB losses),  $\alpha = 3.5$ .

The filter is stationary, and  $\Delta(t) = 0$ . The pump parameter threshold value is taken as  $g_{0,\text{thr}} = -\ln \kappa$ . The model [Eqs. (1)–(3)] is numerically integrated by means of an Euler scheme with a step  $dt = 1.05$  ps. The initial condition corresponds to the laser-off state  $E(t < 0) = 0$ ,  $G(t < 0) = g_0$ , and the laser is turned on at the moment  $t = 0$ .

The upper panels of Fig. 2 depict the first ten round trips of the laser turn-on transient observed experimentally (a) and calculated numerically (b). Spontaneous emission,

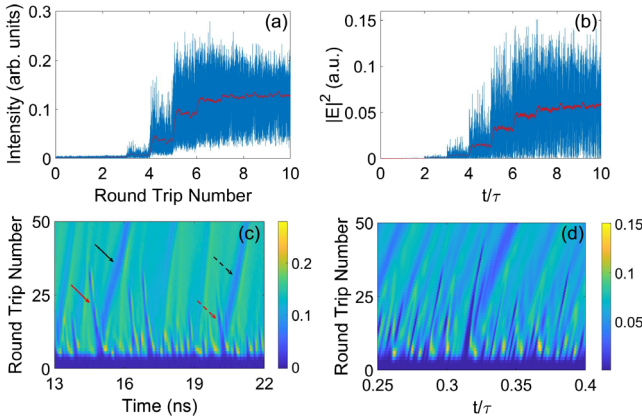


FIG. 2. (a) Experimental time trace of the intensity over the first 10 round trips after the turn-on of the SOA (round trip 0) recorded at 12 GHz bandwidth (blue) and numerically filtered down to 100 MHz (red). (b) The simulated time traces of the laser intensity over the first 10 roundtrips after the pump turn-on: within the full simulation bandwidth (blue) and filtered down to 100 MHz (red). (c) Experimental 2D map of the laser intensity time trace in a 9 ns time window over the first 50 round-trips. The arrows indicate two distinct types of power dropout structures. (d) Numerically calculated evolution of the laser intensity during the first 50 round-trips.

emitted by the SOA as soon as the pump current increases, is reamplified after each round trip. As a result, the laser intensity, averaged over one round-trip, increases in a stepwise fashion and reaches its steady-state value after a few round-trips. The laser continues to exhibit large amplitude fluctuations for a much longer duration, and, to obtain further insights on this dynamics, we represent the evolution of the laser output in the first 50 round-trips by using spatiotemporal diagrams [21], as shown in Figs. 2(c) and 2(d). These diagrams allow one to visualize the evolution round-trip after round-trip of the intensity in a time window [9 ns in panel (b)] shorter than the cavity round-trip time. Figure 2(c) reveals the existence of two types of power dropouts. The first type (indicated by red arrows) appears within the first round-trips of the turn-on transient and disappears after about 25 round-trips. The second type of power dropouts (indicated by black arrows) remains for a much greater number of round-trips, and it features a periodicity larger than the first type of dropouts. This implies that the first type of dropouts has a larger group velocity than the second type. The formation of these power dropouts, which characterizes the initial stage of the switch-on transient, is reproduced numerically by integrating Eqs. (1)–(3), as shown in the spatiotemporal diagrams of Fig. 2(d).

The initial stage of the long-cavity laser switch on can be described as an iterative process of noise regeneration. The intracavity filter bandwidth determines the bandwidth of the thermal noise initial condition. After each round-trip, the statistical fluctuations are modified as the laser intensity is reamplified. To describe this behavior, one can reduce Eqs. (1)–(3) to a one-dimensional map describing the evolution of the laser intensity after each round-trip (see Sec. I of the Supplemental Material [33])  $p_n = |E(n\tau)|^2$ ,

$$p_n = \kappa \exp\left(\frac{g_0}{1 + p_{n-1}}\right) p_{n-1}. \quad (4)$$

The evolution of the laser intensity probability distribution functions (PDF) during the laser switch on can be calculated from numerical and experimental data, and it is shown in Fig. 3. The evolution of these PDFs shows a similar behavior as observed in the switch on of a single longitudinal mode laser [8,34], as they display a conventional thermal statistics for the first round-trips before developing a broad bell-shaped distribution (16th round-trip). On the other hand, the PDF shown in Fig. 3 exhibits a long tail toward the low intensities due to the existence of the persisting power dropouts.

To gain further insight about the role of these long lasting dropouts, we measured the temporal evolution of the electric field [31] during the turn-on transient. Figure 4 shows the temporal evolution of the laser intensity and electric field within a 20 ns time window at the round-trip numbers 5, 15, and 500. These time series are obtained

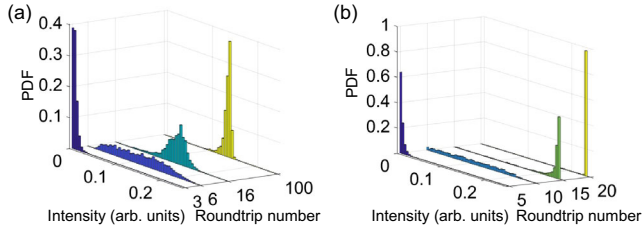


FIG. 3. Experimental (a) and numerical (b) probability distributions of the laser intensity for successive round-trips during the laser turn-on. Numerical histograms are obtained with the 1D intensity map.

from the switch-on realization depicted in Fig. 2, and the time window at different round-trips has been centered around the power dropout identified by the left black arrow in Fig. 2(c) and, correspondingly, in Fig. 4(b).

During the 5th round-trip, the intensity fluctuates near its mean value while the electric field exhibits large and aperiodic variations, indicating that the optical phase is widely fluctuating. At the 15th round-trip, the electric field displays a periodic evolution with small phase discontinuities near the dropout marked by the arrow. At round-trip number 500, we observe that the electric field tends toward a sinusoidal evolution, but a phase discontinuity is observed in correspondence to the power dropout which now exhibits a larger amplitude. Measurements of the optical frequency around this power dropout (see Fig. 2 in the Supplemental Material [33]) demonstrate that it connects monochromatic domains of laser emission with slightly different frequencies. Hence, the dropout observed in Fig. 4(c) can be interpreted as analogous to a source of traveling waves observed in spatially extended systems and

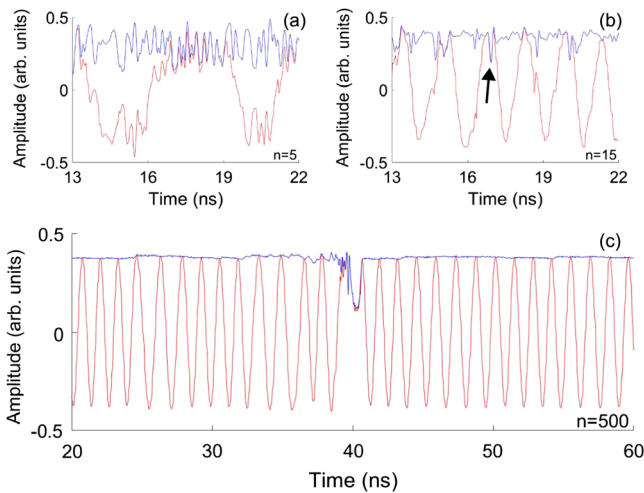


FIG. 4. Experimental time traces of the laser electric field (red) and intensity (blue) at round trips 5 (a), 15 (b), and 500 (c). The arrow in panel b indicates the position of the dropout marked by the left black arrow in Fig. 2(c) appearing during the first round trips.

described within the framework of the complex Ginzburg-Landau equation [18].

The behavior of these holes depends on the dispersion and pump power, and it can also vary from one realization of the laser switch-on to another, as illustrated in Fig. 5. The first two panels describe two different realizations obtained for the same parameters: no hole is originated in panel (a), while, in panel (b), a hole is seeded by a long lasting dropout appearing during the initial stage of the switch-on. We note that, when the dropout evolves into a hole (round-trip number 300), its amplitude increases, and its group velocity abruptly decreases. A close look at the evolution of the hole reveals that, as described in Ref. [35], it emits bursts that propagate at a faster group velocity than the hole and that decay in the neighborhood of the hole.

For lower injection current, we observe that more power dropouts persist and seed several holes, as described in Fig. 5(c). The dynamics of each hole is similar to that observed at higher injection current, i.e., it emits intensity bursts which travel at larger speed. In this regime, these bursts do not interact with other holes as they decay rapidly as soon as they are ejected from the holes. The situation is drastically modified when the laser is operated in the anomalous dispersion regime (the intracavity filter is set at 1360 nm), as illustrated in Fig. 5(d). In this regime, the number of power dropouts per round-trip is much larger, and the radiation emitted from each hole reaches and modifies the dynamics of the preceding hole, thus leading to a chaotic trajectory of the hole core. Such a behavior constitutes, to our knowledge, a new type of dynamics in defect-mediated turbulence [36].

To quantify the degree of decoherence induced by such dynamics, we compute the coherence time as a function of

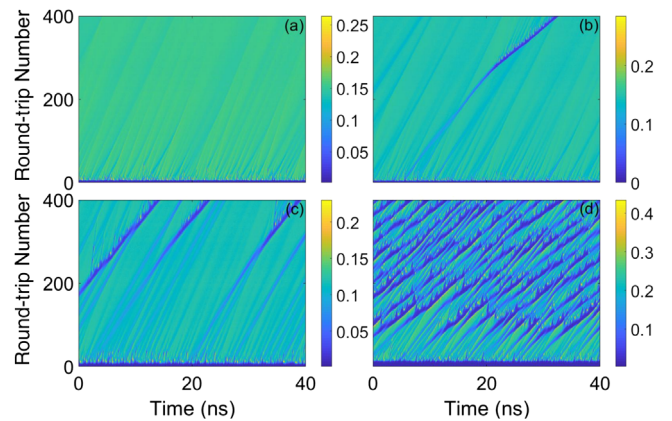


FIG. 5. Maps of the laser intensity for different pump power and operating wavelength. (a),(b) Two different transient build-ups obtained for  $P = 1.6 * P_{th}$ , operating at 1310 nm (normal dispersion). (c)  $P = 1.2 * P_{th}$ , filter at 1310 nm (normal dispersion). (d)  $P = 1.2 * P_{th}$ , filter at 1360 nm (anomalous dispersion).

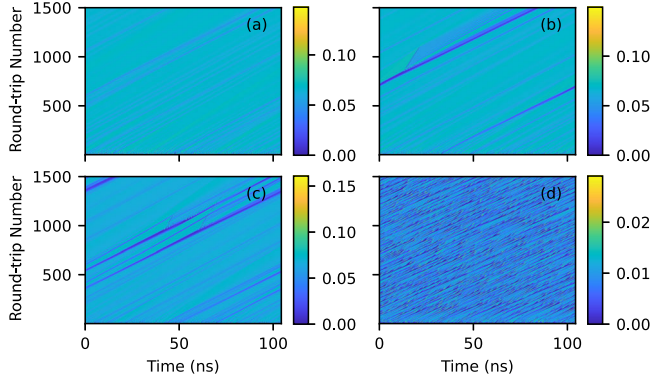


FIG. 6. Numerical maps of the laser intensity obtained by numerical integration of Eqs. (1)–(3) to match the experimental data shown in Fig. 5. The maps are computed for a zero-dispersion regime ( $\epsilon = 0$ ) with  $g_0 = 1.6g_{0,\text{thr}}$  (a),(b),  $g_0 = 1.2g_{0,\text{thr}}$  (c), and anomalous dispersion regime (d) with  $g_0 = 1.2g_{0,\text{thr}}$ ,  $\epsilon = 1.6$ ,  $\Omega = 30.4$  GHz, and  $\Gamma = 15.2$  GHz. The other parameters are the same as in the main text.

the round-trip number for each situation shown in Fig. 5. The coherence time per round-trip is obtained by integrating the optical power spectrum [37]:

$$\tau_c = \frac{\int_{-\infty}^{+\infty} |S(\nu)|^2 d\nu}{\left(\int_{-\infty}^{+\infty} |S(\nu)| d\nu\right)^2}, \quad (5)$$

where  $|S(\nu)|$  is the optical power spectral density computed using the fast Fourier transform of the complex electric field that was retrieved by means of the interferometric technique in the experiment.

We see from Figs. 6 and 7 that the model [Eqs. (1)–(3)] is able to quantitatively retrieve the experimental results. In Fig. 6 numerical maps of laser intensity illustrating transient buildups are shown in zero (a)–(c) and anomalous (d) dispersion regimes. They are in agreement with the experimental data shown in Fig. 5. Figure 7 shows that the coherence time quickly increases during the first 30 round-trips, which confirms the observations made earlier. Afterward we may distinguish between three types of behavior. In the case where the transient results in no drop or a single drop (blue and orange curves respectively), we observe that the coherence time converges to a value of about 3 nanoseconds after approximately 500 round-trips. In the multiple drops case (green curve), we notice a decrease in the coherence time with respect to the former cases. This can be explained by the collisions experienced by the multiple coherent structures present in the round-trip. These collisions occur at random times, which explains why the green curves in Fig. 7 show large fluctuations either experimentally or numerically. The amplitude of the fluctuations of the coherence time is visible in Fig. 4 of the Supplemental Material [33], where we have computed the average coherence time and standard deviation over 21 realizations with different initial

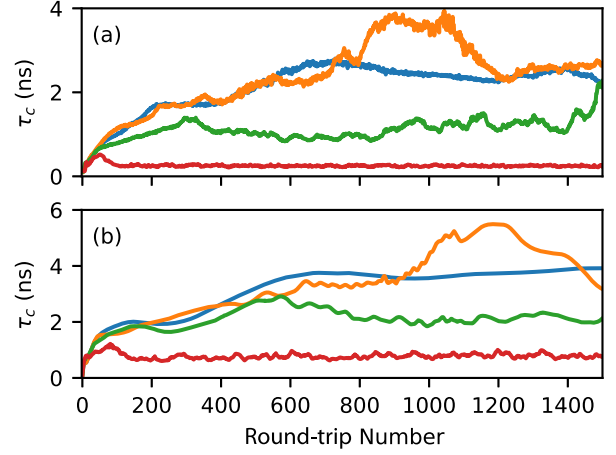


FIG. 7. Coherence times  $\tau_c$  as a function of the round-trip number. (a) Experiment. Transient resulting in no drop (blue) corresponding to the situation shown in Fig. 5(a), single drop (orange) corresponding to the situation shown in Fig. 5(b), multiple drops (green) corresponding to the situation shown in Fig. 5(c), defect-mediated turbulence in the anomalous dispersion regime (red) corresponding to the situation shown in Fig. 5(d). (b) Theory. Coherence times are calculated for simulated transients that are identical to the experimental ones in Fig. 6.

conditions for the “multiple drops” case (green curve). Finally, the situation is drastically modified in the anomalous dispersion regime. In fact, we observe that, after a rapid increase in the first round-trips, the experimentally measured coherence time decreases and reaches the limit of about 100 ps corresponding to the inverse of the filter bandwidth. Although the dynamics of the laser is highly multimode in this situation, the coherence time remains remarkably constant with a further increase of the round-trip number. This experimental observation is well reproduced by the numerical analysis.

In conclusion, we have presented a round-trip-resolved evolution of the intensity and phase during the turn-on of a long laser which has allowed us to disclose the universal mechanisms at the origin of coherent structures and turbulence. We have demonstrated that the transition from thermal to Poisson statistics in the first round-trips is closely connected to the existence of power dropouts. These dropouts can survive after multiple round-trips and seed coherent structures or holes. These structures emit intensity bursts that propagate at faster group velocity than the holes. Turbulence arises in the anomalous dispersion regime via the multiple collisions between these bursts and other holes, thus acting as a temporal decoherence mechanism. Our results provide, to our knowledge, the first detailed investigation of the transient evolution of a dynamical system toward coherent structures and turbulent states. Beyond long cavity lasers, our findings may be relevant to a large class of dynamical systems in nature.

We acknowledge funding from the European Commission for the projects H2020-MSCA-IF-2017, ICOFAS (800290), and H2020-MSCA-RISE-2018 HALT, from the Munster Technological University for funding of A. R.'s PhD Scholarship 2018; Région PACA for the OPTIMAL project; Ministry of Science and Higher Education of the RF (Grant No. 2019-1442/Ref. No. FSER-2020-0013); Deutsche Forschungsgemeinschaft (DFG Project No. 445430311). The authors declare no conflicts of interest.

- 
- [1] P. Sharma, S. Pardeshi, R. K. Arora, and M. Singh, A review of the development in the field of fiber optic communication systems, *Int. J. Emerging Technol. Adv. Eng.* **3**, 113 (2013).
- [2] W. Drexler and J. G. Fujimoto, *Optical Coherence Tomography* (Springer, Berlin, 2015).
- [3] R. Holzwarth, T. Udem, T. W. Haensch, J. Knight, W. Wadsworth, and P. S. J. Russell, Optical Frequency Synthesizer for Precision Spectroscopy, *Phys. Rev. Lett.* **85**, 2264 (2000).
- [4] A. D. V. Di Virgilio, A. Basti, N. Beverini, F. Bosi, G. Carelli, D. Ciampini, F. Fuso, U. Giacomelli, E. Maccioni, P. Marsili, A. Ortolan, A. Porzio, A. Simonelli, and G. Terreni, Underground Sagnac gyroscope with sub-prad/s rotation rate sensitivity: Toward general relativity tests on Earth, *Phys. Rev. Res.* **2**, 032069(R) (2020).
- [5] S. Capozziello, C. Altucci, F. Bajardi, A. Basti, N. Beverini, G. Carelli, D. Ciampini, A. D. V. Di Virgilio, F. Fuso, U. Giacomelli, E. Maccioni, P. Marsili, A. Ortolan, A. Porzio, A. Simonelli, G. Terreni, and R. Velotta, Constraining theories of gravity by GINGER experiment, *Eur. Phys. J. Plus* **136**, 294 (2021).
- [6] A. D. D. Virgilio, C. Altucci, F. Bajardi, A. Basti, N. Beverini, S. Capozziello, G. Carelli, D. Ciampini, F. Fuso, U. Giacomelli, E. Maccioni, P. Marsili, A. Ortolan, A. Porzio, A. Simonelli, G. Terreni, and R. Velotta, Sensitivity limit investigation of a Sagnac gyroscope through linear regression analysis, *Eur. Phys. J. C* **81**, 400 (2021).
- [7] R. Loudon, *The Quantum Theory of Light* (Oxford University Press, Oxford, 2000).
- [8] F. T. Arecchi, V. Degiorgio, and B. Querzola, Time-Dependent Statistical Properties of the Laser Radiation, *Phys. Rev. Lett.* **19**, 1168 (1967).
- [9] A. L. Schawlow and C. H. Townes, Infrared and optical masers, *Phys. Rev.* **112**, 1940 (1958).
- [10] T. Wang, D. Aktas, O. Alibart, É. Picholle, G. P. Puccioni, S. Tanzilli, and G. L. Lippi, Superthermal-light emission and nontrivial photon statistics in small lasers, *Phys. Rev. A* **101**, 063835 (2020).
- [11] P. R. Rice and H. J. Carmichael, Photon statistics of a cavity-QED laser: A comment on the laser-phase-transition analogy, *Phys. Rev. A* **50**, 4318 (1994).
- [12] E. Turitsyna, S. Smirnov, S. Sugavanam, N. Tarasov, X. Shu, S. Babin, E. Podivilov, D. Churkin, G. Falkovich, and S. Turitsyn, The laminar-turbulent transition in a fibre laser, *Nat. Photonics* **7**, 783 (2013).
- [13] D. Tang, J. Guo, Y. Song, H. Zhang, L. Zhao, and D. Shen, Dark soliton fiber lasers, *Opt. Express* **22**, 19831 (2014).
- [14] D. Churkin, S. Sugavanam, N. Tarasov, S. Khorev, S. Smirnov, S. Kobtsev, and S. Turitsyn, Stochasticity, periodicity and localized light structures in partially mode-locked fibre lasers, *Nat. Commun.* **6**, 7004 (2015).
- [15] S. Slepneva, B. O'Shaughnessy, A. G. Vladimirov, S. Rica, E. A. Viktorov, and G. Huyet, Convective Nozaki-Bekki holes in a long cavity OCT laser, *Opt. Express* **27**, 16395 (2019).
- [16] M. Piccardo, B. Schwarz, D. Kazakov, M. Beiser, N. Opačak, Y. Wang, S. Jha, J. Hillbrand, M. Tamagnone, W. T. Chen, A. Y. Zhu, L. L. Columbo, A. Belyanin, and F. Capasso, Frequency combs induced by phase turbulence, *Nature (London)* **582**, 360 (2020).
- [17] N. Opačak, D. Kazakov, L. L. Columbo, M. Beiser, T. P. Letsou, F. Pilat, M. Brambilla, F. Prati, M. Piccardo, F. Capasso, and B. Schwarz, Nozaki-Bekki optical solitons, [arXiv:2304.10796](https://arxiv.org/abs/2304.10796).
- [18] I. S. Aranson and L. Kramer, The world of the complex Ginzburg-Landau equation, *Rev. Mod. Phys.* **74**, 99 (2002).
- [19] R. Lang and K. Kobayashi, External optical feedback effects on semiconductor injection laser properties, *IEEE J. Quantum Electron.* **16**, 347 (1980).
- [20] A. G. Vladimirov and D. Turaev, Model for passive mode locking in semiconductor lasers, *Phys. Rev. A* **72**, 033808 (2005).
- [21] G. Giacomelli and A. Politi, Relationship Between Delayed and Spatially Extended Dynamical Systems, *Phys. Rev. Lett.* **76**, 2686 (1996).
- [22] M. Marconi, J. Javaloyes, S. Balle, and M. Giudici, How Lasing Localized Structures Evolve Out of Passive Mode Locking, *Phys. Rev. Lett.* **112**, 223901 (2014).
- [23] A. G. Vladimirov, A. V. Kovalev, E. A. Viktorov, N. Rebrova, and G. Huyet, Dynamics of a class-A nonlinear mirror mode-locked laser, *Phys. Rev. E* **100**, 012216 (2019).
- [24] S. Yanchuk, S. Ruschel, J. Sieber, and M. Wolfrum, Temporal Dissipative Solitons in Time-Delay Feedback Systems, *Phys. Rev. Lett.* **123**, 053901 (2019).
- [25] M. Wolfrum and S. Yanchuk, Eckhaus Instability in Systems with Large Delay, *Phys. Rev. Lett.* **96**, 220201 (2006).
- [26] A. Pimenov, S. Slepneva, G. Huyet, and A. G. Vladimirov, Dispersive Time-Delay Dynamical Systems, *Phys. Rev. Lett.* **118**, 193901 (2017).
- [27] I. Yarutkina, O. Shtyrina, M. Fedoruk, and S. Turitsyn, Numerical modeling of fiber lasers with long and ultra-long ring cavity, *Opt. Express* **21**, 12942 (2013).
- [28] R. Huber, M. Wojtkowski, and J. Fujimoto, Fourier domain mode locking (FDML): A new laser operating regime and applications for optical coherence tomography, *Opt. Express* **14**, 3225 (2006).
- [29] S. Slepneva, B. Kelleher, B. O'Shaughnessy, S. Hegarty, A. Vladimirov, and G. Huyet, Dynamics of Fourier domain mode-locked lasers, *Opt. Express* **21**, 19240 (2013).
- [30] K. Nozaki and N. Bekki, Exact solutions of the generalized Ginzburg-Landau equation, *J. Phys. Soc. Jpn.* **53**, 1581 (1984).
- [31] B. Kelleher, D. Goulding, a. H. S. Pascual, Beatrice, and G. Huyet, Phasor plots in optical injection experiments, *Eur. Phys. J. D* **58**, 175 (2010).
- [32] A. Pimenov, S. Amiranashvili, and A. G. Vladimirov, Temporal cavity solitons in a delayed model of a dispersive cavity ring laser, *Math. Model. Nat. Phenom.* **15**, 47 (2020).

- [33] See Supplemental Material at <http://link.aps.org/supplemental/10.1103/PhysRevLett.131.053801> for additional theoretical and experimental analysis and figures.
- [34] H. Risken and H. Vollmer, The transient solution of the laser Fokker-Planck equation, *Z. Phys. A Hadrons Nucl.* **204**, 240 (1967).
- [35] U. Gowda, A. Roche, A. Pimenov, A. G. Vladimirov, S. Slepneva, E. A. Viktorov, and G. Huyet, Turbulent coherent structures in a long cavity semiconductor laser near the lasing threshold, *Opt. Lett.* **45**, 4903 (2020).
- [36] P. Couillet, L. Gil, and J. Lega, Defect-Mediated Turbulence, *Phys. Rev. Lett.* **62**, 1619 (1989).
- [37] T. Butler, S. Slepneva, B. O'shaughnessy, B. Kelleher, D. Goulding, S. P. Hegarty, H.-C. Lyu, K. Karnowski, M. Wojtkowski, and G. Huyet, Single shot, time-resolved measurement of the coherence properties of OCT swept source lasers, *Opt. Lett.* **40**, 2277 (2015).